Image Anal Stereol 2023;42:119-132 doi: 10.5566/ias.2917
Original Research Paper

MAGNETIC RESONANCE IMAGE DENOISING BASED ON LAPLACIAN PRIOR SPARSITY CONSTRAINT AND NONCONVEX SECOND-ORDER TV PENALTY

YUMENG GE[1,2], WEI XUE[✉,1,2], YUN XU[1,2], JUN HUANG[1,2] AND XIAOLEI GU[3]

[1]School of Computer Science and Technology, Anhui University of Technology, Maanshan 243032, China,
[2]Institute of Artificial Intelligence, Hefei Comprehensive National Science Center, Hefei 230088, China,
[3]Department of Radiology, Maanshan People's Hospital, Maanshan 243099, China
e-mail: geyumeng2@foxmail.com; xuewei@ahut.edu.cn; zxy411killer@gmail.com; huangjun.cs@ahut.edu.cn; guxiaolei88@sina.com
(Received April 22, 2023; accepted June 29, 2023)

ABSTRACT

Magnetic resonance (MR) imaging is considered as a very powerful imaging modality in clinical examination, but the process of image acquisition and transmission will be affected by noise, resulting in the degradation of imaging quality. In this paper, based on the Laplacian prior sparsity constraint and the nonconvex second-order total variation (TV) penalty, we propose a MR images denoising model which consists of three terms. Specifically, in the first term, we use the L_2-norm as the fidelity term to control the proximity between the observed image and the recovered MR image. Then, we introduce the Laplacian sparse prior constraint as the second term to mitigate the staircase artifacts in the recovered image. In the third term, we adopt the nonconvex second-order TV penalty to preserve important textures and edges. Finally, we use the alternating direction method of multipliers to solve the corresponding minimization problem. Comparative experiments on clinical data demonstrate the effectiveness of our approach in terms of PSNR and SSIM values.

Keywords: image denoising, Laplacian prior, magnetic resonance imaging, second-order total variation, sparsity constraint.

INTRODUCTION

MR imaging is a remarkable imaging technology that provides highly detailed images of human tissues and organs. It is mainly used to demonstrate pathological or other physiological changes in living tissues (Mohan *et al.*, 2014). The visual quality of MR images plays an important role in the accuracy of clinical diagnosis. However, MR images are susceptible to noise corruption during image acquisition and transmission, which can degrade the image quality and hinder the effective feature extraction, recognition, and analysis. Therefore, for clinical diagnosis, the recovery value of MR images is of significant importance.

Many methods have been proposed for MR images denoising, such as wavelet transform, partial differential equation, and TV regularization. First of all, the usage of wavelets in MR images denoising was pioneered by Weaver *et al.* (1991), which used the wavelet transform instead of the Fourier transform to reduce noise from 10% to 50%. In order to denoise brain imaging resonances used for medical purposes, (Sonia and Sumathi, 2022) analyzed the effectiveness of various wavelet-based thresholding methods in the presence of scattered noise for different wavelet families including Morlet, Symlet, Daubechies, and Haar. Al-Shayea *et al.* (2020) proposed a four-level discrete wavelet transform medical image denoising algorithm that utilized different wavelet families and median filtering to remove Gaussian noise from multiple medical images.

There exist some denoising methods that are based on partial differential equations (PDE). In (El Hakoume *et al.*, 2022), an improved coupled PDE denoising model based on diffusion tensor was proposed, which was more suitable for representing small details in texture images. Hadri *et al.* (2021) investigated a novel PDE constraint optimization model with discontinuous variable indices for the removal of different noise types from MR images. Tong *et al.* (2012) proposed a scheme for anisotropic diffusion filtering of MR images, an automatic parameter selection method to obtain better denoising results.

In addition to the above methods, this paper mainly considers the denoising method based on the TV regularization. Rudin *et al.* (1992) first proposed the Rudin-Osher-Fatemi model based on TV, which can preserve edges and remove image noise in homogeneous regions. In this method, the noisy image is represented as $g = f + n$, where f denotes the

original clean image and n denotes the noise. In order to reconstruct f from g, the corresponding minimization problem is formulated as

$$\min_f \frac{1}{2}||g-f||_2^2+\lambda\phi_{TV}(f), \tag{1}$$

where $||.||_2$ denotes the Euclidean norm, $\lambda > 0$ is the regularization parameter, $\phi_{TV}(f)$ is the TV regularization function denoted as $\phi_{TV}(f) = \sum_{i,j=1}^{n}||(\nabla f)_{i,j}||_1$ and the discrete gradient operator $\nabla : R^{n^2} \to R^{2\times n^2}$ is defined by $(\nabla f)_{i,j} = ((\nabla_x f)_{i,j},(\nabla_y f)_{i,j})$ with

$$(\nabla_x f)_{i,j} = \begin{cases} f_{i+1,j}-f_{i,j}, & \text{if} \quad i<n, \\ f_{1,j}-f_{n,j}, & \text{if} \quad i=n, \end{cases}$$

and,

$$(\nabla_y f)_{i,j} = \begin{cases} f_{i,j}-f_{i,j+1}, & \text{if} \quad j<n, \\ f_{i,1}-f_{i,n}, & \text{if} \quad j=n. \end{cases}$$

for i, j=1, $\cdots$, n, where $f_{i,j}$ refers to the $((j-1)n+i)$-th entry of the vector f [1].

However, traditional TV regularizations may lead to staircase artifacts. To mitigate staircase artifacts, Liu *et al.* (2015b) proposed the overlapping group sparsity total variation (OGSTV) image restoration model. Further, (Shi *et al.*, 2016) proposed a model that combines OGSTV and hyper-Laplacian prior. New regularizations have been proposed for the hyper-Laplacian prior with OGSTV, integrating pixel-level and structural sparseness of natural image gradient (Jon *et al.*, 2021a;b). Adam and Paramesran (2019) combined the overlapping group sparsity regularization with nonconvex high-order TV, and the proposed model has the advantages of both the overlapping group sparsity regularization smoothing staircase artifacts and nonconvex high-order TV preserving sharp edges. There are also many TV methods applied to MR images. For example, integrating TV denoising, curvilinear wave denoising, and edge information has been shown to significantly improve the noise suppression of medical images (Bhadauria and Dewal, 2013). Snehalatha (2020) proposed a spectral TV algorithm to denoise brain MR images while preserving edges. In (Zhu *et al.*, 2020), an improved TV algorithm was proposed for removing Gaussian noise in compression-sensing MR images reconstruction. Gu *et al.* (2023) proposed a new MRI image recovery model combining least absolute deviations measure and isotropic total variation, which can effectively suppress noise and preserve image smoothness.

According to the literature survey, it is found that most of the existing methods mainly focus on alleviating the staircase effect, ignoring the texture and edge of the image. In order to further improve the denoising performance of the model based on TV, we propose a MR images denoising method that combines the hyper-Laplacian prior regularization with OGSTV and nonconvex second-order TV. The proposed method takes into account the gradient distribution and structural information of MR images to reduce staircase artifacts, while also preserving local textures and edges through nonconvex second-order terms. Due to the computational problems caused by the complexity of the model, we use the alternate direction multiplier algorithm to solve the subproblems. Finally, we conduct numerical experiments to analyze the effectiveness of the proposed model.

The rest of this paper is organized as follows. In Section 2, we introduce the basic concepts of the proposed regularization and briefly review overlapping group sparsity, hyper-Laplacian priors, and alternating direction method of multipliers (ADMM). In Section 3, we propose a new model for image denoising and derive an efficient algorithm to solve the corresponding minimization problem. In section 4, the superiority of the proposed method is proved by numerical experiments. Finally, a conclusion is made in Section 5.

PRELIMINARIES

To provide a more comprehensive description of the model, this section introduces three key components: the overlapping group sparsity prior, the hyper-Laplace prior, and the ADMM framework.

OVERLAPPING GROUP SPARSITY PRIOR

In (Selesnick and Chen, 2013), the OGSTV has been used to solve the problem of one-dimensional signal denoising, which could effectively alleviate staircase artifacts. Liu *et al.* (2015a;b) extended the OGSTV function to the general two-dimensional case as a new regularization, then they defined a $K\times K$ point group of the image $g \in \mathbb{R}^{n^2}$

[1] $f_{i,j}$ is the (i,j)-th pixel location of the $n\times n$ image, and this notation remains valid throughout the paper unless otherwise specified

$$\tilde{g}_{i,j,k} = \begin{bmatrix} g_{i-m_l,j-m_l} & g_{i-m_l,j-m_l+1} & \cdots & g_{i-m_l,j+m_r} \\ g_{i-m_l+1,j-m_l} & g_{i-m_l+1,j-m_l+1} & \cdots & g_{i-m_l+1,j+m_r} \\ \vdots & \vdots & \ddots & \vdots \\ g_{i+m_r,j-m_l} & g_{i+m_r,j-m_l+1} & \cdots & g_{i+m_r,j+m_r} \end{bmatrix} \in \mathbb{R}^{K\times K}, \tag{2}$$

where $m_l = \lfloor \frac{K-1}{2} \rfloor$, $m_r = \lfloor \frac{K}{2} \rfloor$, and $\lfloor x \rfloor$ denotes the largest integer which less than or equal to x. The center of $\tilde{g}_{i,j,k}$ is located at (i,j), and $g_{i,j,k}$ is a vector obtained by stacking the k columns of the matrix $\tilde{g}_{i,j,k}$, i.e., $g_{i,j,k} = \tilde{g}_{i,j,k}(:)$. Then the overlapping group sparsity regularization can be defined as follows

$$\phi_{OT}(g) = \sum_{i,j+1} ||g(i,j)_K||_2. \tag{3}$$

HYPER-LAPLACIAN PRIOR

Recent studies have shown that the hyper-Laplacian prior can well approximate the heavy-tailed distribution of gradients in natural scenes (Krishnan and Fergus, 2009; Chang *et al.*, 2017; Kong *et al.*, 2017). Moreover, the heavy-tailed distribution has also been observed in MR images (Liu *et al.*, 2014). The corresponding hyper-Laplacian image prior can be modeled as follows

$$p(f) \propto \quad \prod_{i,j}^{n} e^{-||\nabla f||_q^q}, \tag{4}$$

where $||.||_q$ denotes quasi-norm l_q with $0 < q < 1$, namely, $||(\nabla f)_{i,j}||_q^q = |(\nabla_x f)_{i,j}|^q + |(\nabla_y f)_{i,j}|^q$. Due to the nonconvexity of l_q in

$$\phi_{HL}(f) = \sum_{i,j=1}^{n} ||(\nabla f)_{i,j}||_q^q. \tag{5}$$

In (Jon *et al.*, 2021b), the overlapping group sparsity also represents the hyper-Laplacian prior, and the experimental results show that it can improve the quality of the recovered image. Therefore, the overlapping group sparsity regularization on hyper-Laplacian prior (OGS-HL) is proposed for image denoising and deblurring. The OGS-HL regularization $\phi_{OH}(g)$ is defined as follows

$$\Phi_{OH}(g) = \sum_{i,j=1}^{n} |||g_{(i,j),k}|^q||_2 = \sum_{i,j=1}^{n} \sqrt{\sum_{k_1,k_2=-m_l}^{m_r} |g_{i+k_1,j+k_2}|^{2q}}, \tag{6}$$

where $|\cdot|^q$ is the absolute value of the q-th power. It is worth noting that $\Phi_{OH}(g)$ reduces to $\phi_{HL}(f)$ when K= 1, and to $\phi_{OT}(g)$ when $q = 1$. However, $\Phi_{OH}(g)$ is generally nonconvex.

ADMM

The ADMM is a computational framework for solving optimization problems. It decomposes the original optimization problem into several subproblems that are iteratively solved. ADMM is particularly useful for solving constrained separable optimization problems of the form:

$$\begin{aligned} &\min_{x_1,x_2} \xi_1(x_1) + \xi_2(x_2) \\ &\text{s.t.} \quad Ax_1 + Bx_2 = d, \\ &x_i \in \chi_i, \quad i = 1,2 \end{aligned} \tag{7}$$

where $\xi_i(\cdot) : \chi_i \to \mathbb{R}$ are closed convex functions, $A, B \in \mathbb{R}^{l\times n}$, $d \in \mathbb{R}^l$ is a given vector. The augmented Lagrangian function (Hestenes, 1969) for the problem (7) is defined as

$$\begin{aligned} \mathscr{L}_{\mathscr{A}}(x_1,x_2;\mu) =& \xi_1(x_1) + \xi_2(x_2) + \mu^T(Ax_1 + Bx_2 - d) \\ &+ \frac{\delta}{2}||Ax_1 + Bx_2 - d||_2^2, \end{aligned} \tag{8}$$

where $\mu \in \mathbb{R}^l$ is the Lagrange multiplier and $\delta > 0$ is a penalty parameter. The objective is to find the saddle point of $\mathscr{L}_{\mathscr{A}}$ by alternatively minimizing $\mathscr{L}_{\mathscr{A}}$ with respect to x_1, x_2 and μ. The ADMM algorithm to solve the problem (7) is presented as Algorithm 1.

Algorithm 1 ADMM for minimizating the problem (7).

1: initialization x_1^0, x_2^0, λ^0 and $\delta > 0$,
2: iteration:
$x_1^{k+1} = \arg\min_{x_1} \xi_1(x_1) + \frac{\delta}{2}||Ax_1 + Bx_2^k - d + \frac{\mu^k}{\delta}||_2^2$,
$x_2^{k+1} = \arg\min_{x_2} \xi_2(x_2) + \frac{\delta}{2}||Ax_1^{k+1} + Bx_2 - d + \frac{\mu^k}{\delta}||_2^2$,
$\mu^{k+1} = \mu^k + \delta(Ax_1^{k+1} + Bx_2^{k+1} - d)$,
$k = k+1$
3: until a stopping criterion is satisfied.

PROPOSED ALGORITHM

In this section, we first present the proposed MR image denoising model, followed by its solution using the ADMM framework.

MODEL

The proposed MR image denoising model is of the form

$$\min_f \frac{\lambda}{2}||g-f||_2^2+\Phi(\nabla f)+\alpha||\nabla^2 f||_p^p, \tag{9}$$

where λ, $\alpha>0$ are regularization parameters that controls the data fidelity term and the nonconvex second order regularization respectively.

OPTIMIZATION

To solve Eq. (9), we transform the original problem into the following constrained optimization problem by introducing two auxiliary variables x_1 and x_2

$$\begin{aligned}&\min_f \frac{\lambda}{2}||g-f||_2^2+\Phi(\nabla f)+\alpha||\nabla^2 f||_p^p,\\ &s.t. x_1=\nabla f, x_2=\nabla^2 f.\end{aligned} \tag{10}$$

To solve (10), we adopt ADMM (Boyd *et al.*, 2011; Wang *et al.*, 2019) and transform Eq. (10) into the following augmented Lagrangian function

$$\begin{aligned}\mathscr{L}_{\mathscr{A}}(f,x_1,x_2;\mu,\delta)&=\frac{\lambda}{2}||g-f||_2^2+\Phi(\nabla f)+\alpha||\nabla^2 f||_p^p\\ &-\mu_1^T(x_1-\nabla f)+\frac{\delta}{2}||x_1-\nabla f||_2^2-\mu_2^T(x_2-\nabla^2 f)\\ &+\frac{\delta}{2}||x_2-\nabla^2 f||_2^2,\end{aligned} \tag{11}$$

where μ_1^T, μ_2^T are Lagrangian multipliers, δ is penalty parameter. To solve Eq. (10), we utilize the ADMM framework and iteratively update each variable by minimizing Eq. (11). This iterative process can be decomposed into several subproblems.

x_1-subproblem

The x_1-subproblem is the overlapping group sparse on the hyper-Laplacian priors problem

$$x_1^{k+1}=\arg\min_{x_1}\frac{\delta}{2}||x_1-(\nabla f^{k+1}+\frac{\mu_1^k}{\delta})||_2^2+\Phi(x_1). \tag{12}$$

The problem (12) can be solved iteratively by the majorization-minimization (MM) algorithm, and the process of solving the related problem is discussed in detail in (Jon *et al.*, 2021b). Here, we express it in lemma 1, as follows:

Lemma 1 *we consider a minimization problem of the form* $\min_v P(v)=\frac{\lambda}{2}||v-v_0||_2^2+\Phi(v)$, *where* λ *is a positive parameter and the functional* $\Phi(v)=\sum_{i,j=1}^n |||g_{(i,j),k}|^q||_2$. *In order to minimize* $P(v)$, *the MM algorithm is continuously iteratively solved to obtain*

$$v^{k+1}=(I+\frac{1}{\lambda}q\Lambda(v^k)^T\Lambda(v^k)R(v^k))^{-1}v_0, \tag{13}$$

where $R(v)=diag(|v|^{2q-2})$.

x_2-subproblem

The x_2-subproblem is a nonconvex denoising problem due to the use of the nonconvex l_p norm second-order regularization

$$x_2^{k+1}=\arg\min_{x_2}\frac{\delta}{2}||x_2-(\nabla^2 f^{k+1}+\frac{\mu_2^k}{\delta})||_2^2+\alpha||x_2||_p^p. \tag{14}$$

Let $y^{k+1}=(\nabla^2 f^{k+1}+\frac{\mu_2^k}{\delta})$, and use the iterative reweighting l_1 (IRL1) algorithm to minimize the problem (14)

$$x_2^{k+1}=\arg\min_{x_2}\frac{1}{2}||x_2-y^{k+1}||_2^2+\sum_i \gamma_i|\beta_i|. \tag{15}$$

The solution to problem (15) is given by the one-dimensional shrinkage function

$$\begin{aligned}x_2^{k+1}&=shrink(y^{k+1},\frac{\gamma_i\alpha}{\delta}),\\ &=max\{|y^{k+1}|-\frac{\gamma_i\alpha}{\delta},0\}\cdot sign(y^{k+1}).\end{aligned} \tag{16}$$

f-subproblem

The f-subproblem

$$\begin{aligned}f^{k+1}=\arg\min_f &\frac{\lambda}{2}||g-f||_2^2-\mu_1^T(x_1-\nabla f)+\frac{\delta}{2}||x_1-\nabla f||_2^2\\ &-\mu_2^T(x_2-\nabla^2 f)+\frac{\delta}{2}||x_2-\nabla^2 f||_2^2,\end{aligned} \tag{17}$$

Subproblem (17) is a least squares problem which is equivalent to the corresponding normal equation

$$\begin{aligned}&(\lambda I+\delta\nabla^T\nabla+\delta(\nabla^2)^T\nabla^2)f\\ &=\lambda g-\nabla^T\mu_1+\delta\nabla^T x_1^k-(\nabla^2)^T\mu_2+\delta(\nabla^2)^T x_2^k.\end{aligned} \tag{18}$$

For the periodic boundary condition of f, $\nabla^T\nabla$ and $(\nabla^2)^T\nabla^2$ are block circulant with circulant blocks, which can be diagonalized by 2D discrete Fourier transform (Wu and Tai, 2010). Therefore, through one FFT operation and one FFT inverse operation, we can

obtain the optimal f as

$$f = \mathscr{F}^{-1}\left(\frac{\mathscr{F}[\lambda g + \delta \nabla^T (x_1^k - \frac{\mu_1}{\delta}) + \delta (\nabla^2)^T (x_2^k - \frac{\mu_2}{\delta})]}{\lambda I + \delta[|\mathscr{F}(\nabla)|^2 + |\mathscr{F}(\nabla^2)|^2]}\right). \tag{19}$$

Updating Lagrangian multiplier

Finally, the Lagrange multipliers are updated by the following

$$\begin{cases} \mu_1^{k+1} = \mu_1^k + (x_1^{k+1} - \nabla f^{k+1}), \\ \mu_2^{k+1} = \mu_2^k + \delta(\nabla^2 f^{k+1} - x_2^{k+1}). \end{cases} \tag{20}$$

We name the proposed method as the Laplacian prior sparsity constraint and nonconvex second-order TV penalty (LAPSTV) algorithm. The LAPSTV algorithm is presented as Algorithm 2. And for this algorithm, we have some remarks.

Algorithm 2 LAPSTV

1: initialization f^0, δ, μ^0, α, K, N, p, q, set $k = 0$,
2: iteration:
Compute x_1^{k+1} according to Eq. (13),
Compute x_2^{k+1} according to Eq. (16),
Compute f^{k+1} according to Eq. (19),
Update μ_i^{k+1}, $i = 1,2$ according to Eq. (20),
$k = k+1$;
3: until a stopping criterion is satisfied.

Remark 1 *In Algorithm 2, we solve the subproblems iteratively in the order of x_1^{k+1}, x_2^{k+1}, f^{k+1}, μ_i^{k+1} ($i = 1,2$). Different orders may yield different denoising results.*

Remark 2 *In the x_2-subproblem, the weight updated at each iteration k in Eq. (15) is given by $\gamma_i = \frac{\alpha p}{(|x_i^k| + \varepsilon)^{1-p}}$, ε is a small number to avoid division by zero. Choosing different weights may affect the denoising results.*

NUMERICAL EXPERIMENTS

In this section, we present several experimental results to verify the effectiveness of the proposed method for image denoising. In Fig. 1, all the test images are from the Department of Radiology, Maanshan People's Hospital, Maanshan, China. The experiment is under Windows 10 and MATLAB R2021a operating system, and the CPU is AMD R7 5800H 3.20GHz and 16GB RAM. MR images used for analysis are corrupted by Gaussian noise with a standard deviation of 15, 20, and 25. All denoising methods measure the quality of recovered images by Peak Signal-to-Noise Ratio (PSNR) and Structural Similarity (SSIM) indices, which reflect human subjective sensory and visual perception quality, respectively (Irum *et al.*, 2015; Zuo *et al.*, 2013).

The stopping criterion for all tested algorithms is set to

$$\frac{||f_{k+1} - f_k||_2}{||f_k||_2} \leq 1 \times 10^{-5}, \tag{21}$$

where f_{k+1} and f_k are the restored image at the current iterate and previous iterate respectively.

RESULTS AND ANALYSIS

We compare our denoising results with two other related methods: OGSTV (Liu *et al.*, 2015b) and HNHOTV-OGS (Adam and Paramesran, 2019). Their regularizations are related to the proposed LAPSTV in this paper.

In the whole experiment, we fix $q = 0.9$, $k = 3$, $N = 5$, $p = 0.1$, and other parameters are manually selected to obtain the most satisfactory restoration quality. For better comparison, the parameters in HNHOTV-OGS are consistent with our method within the range suggested in Adam's paper. For OGSTV, we tune the value of the regularization parameter λ to obtain the best PSNR or SSIM value, while other parameters are the same as suggested in the paper by Liu *et al.*.

The effectiveness of this method on additive Gaussian noise denoising is verified by experiments. Three different noise levels σ = 15, σ = 20, and σ = 25 are added to the test image respectively to generate each observed image. The obtained PSNR and SSIM values are shown in Table 1, Table 2, and Table 3.

In each table, we observe that even at different noise levels, compare with the denoising results of the other two methods, the PSNR and SSIM values of the proposed method were higher. This is because the proposed method combines the advantages of the hyper-Laplacian prior regularization term with overlapping group sparsity and the second-order TV term.

In Fig. 2-4, we present a comparison of the denoised images obtained using three different methods for the MR images of "abdomen" and "pelvic" at σ= 15, "sacroiliac" and "head" at σ=20, and "ankle" and "mrcp" at σ=25, respectively. Based on the obtained results, it can be observed that the denoising effect of the OGSTV method is not optimal, as there are still subtle blocky artifacts present in the denoised images. The most closely

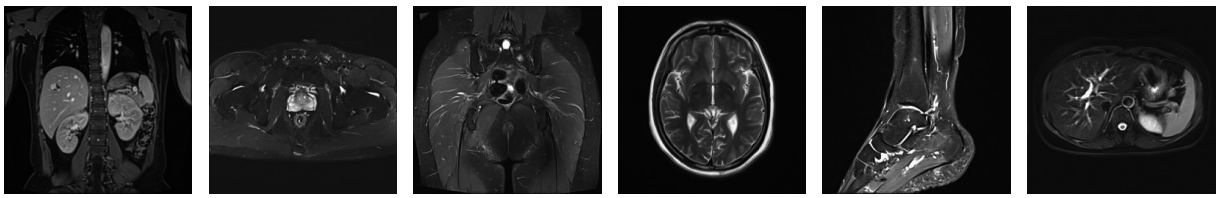

(a) abdomen (b) pelvic (c) sacroiliac (d) head (e) ankle (f) mrcp

Fig. 1: *MR images used for experiments, from left to right, are numbered from (a) to (f).*

Table 1: *The PSNR and SSIM values for denoised images by different methods when* $\sigma = 15$.

σ	Image	Noised	Denoised		
			OGSTV	HNHOTV-OGS	LAPSTV
15	abdomen	24.60/0.447	31.91/0.807	31.54/0.824	**32.65/0.859**
	pelvic	24.60/0.342	31.26/0.755	33.716/0.899	**34.87/0.914**
	sacroiliac	24.60/0.417	31.06/0.770	31.62/0.815	**32.81/0.852**
	head	24.60/0.446	30.77/0.820	32.08/0.929	**33.09/0.942**
	ankle	24.60/0.442	28.20/0.721	31.03/0.907	**32.38/0.928**
	mrcp	24.60/0.359	32.10/0.775	34.04/0.907	**35.03/0.922**

Table 2: *The PSNR and SSIM values for denoised images by different methods when* $\sigma = 20$.

σ	Image	Noised	Denoised		
			OGSTV	HNHOTV-OGS	LAPSTV
20	abdomen	22.10/0.337	30.59/0.763	30.17/0.780	**31.28/0.819**
	pelvic	22.10/0.246	30.01/0.714	32.32/0.880	**33.48/0.894**
	sacroiliac	22.10/0.308	29.83/0.723	30.38/0.780	**31.54/0.819**
	head	22.10/0.357	29.40/0.787	30.35/0.904	**31.43/0.919**
	ankle	22.10/0.350	27.83/0.754	29.36/0.880	**30.77/0.905**
	mrcp	22.10/0.262	30.86/0.737	32.63/0.886	**33.61/0.902**

Table 3: *The PSNR and SSIM values for denoised images by different methods when* $\sigma = 25$.

σ	Image	Noised	Denoised		
			OGSTV	HNHOTV-OGS	LAPSTV
25	abdomen	20.16/0.262	29.67/0.748	29.07/0.724	**30.01/0.763**
	pelvic	20.16/0.187	29.35/0.757	31.44/0.862	**32.37/0.874**
	sacroiliac	20.16/0.236	29.16/0.728	29.50/0.746	**30.45/0.781**
	head	20.16/0.297	27.74/0.791	29.33/0.871	**30.12/0.883**
	ankle	20.16/0.287	26.22/0.754	28.50/0.857	**29.58/0.880**
	mrcp	20.16/0.200	30.22/0.772	31.64/0.865	**32.43/0.879**

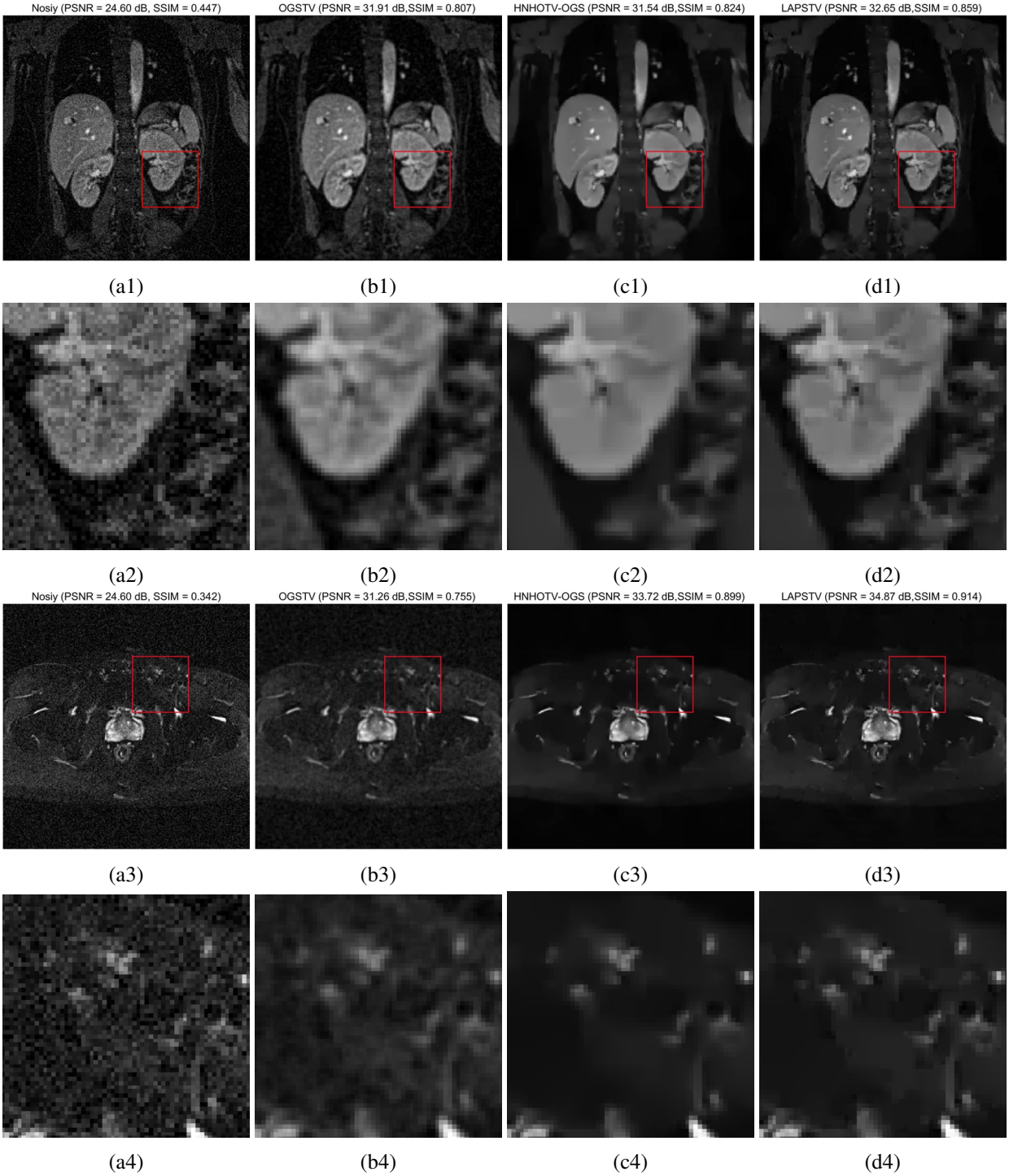

Fig. 2: *The first and third lines are the recovered results for "abdomen" and "pelvic" with* $\sigma = 15$*, respectively, while the second and fourth lines show the fragments corresponding to the zoomed images. (a1)-(a4) noisy image, (b1)-(b4) OGSTV restored, (c1)-(c4) HNHOTV-OGS restored, (d1)-(d4) LAPSTV restored.*

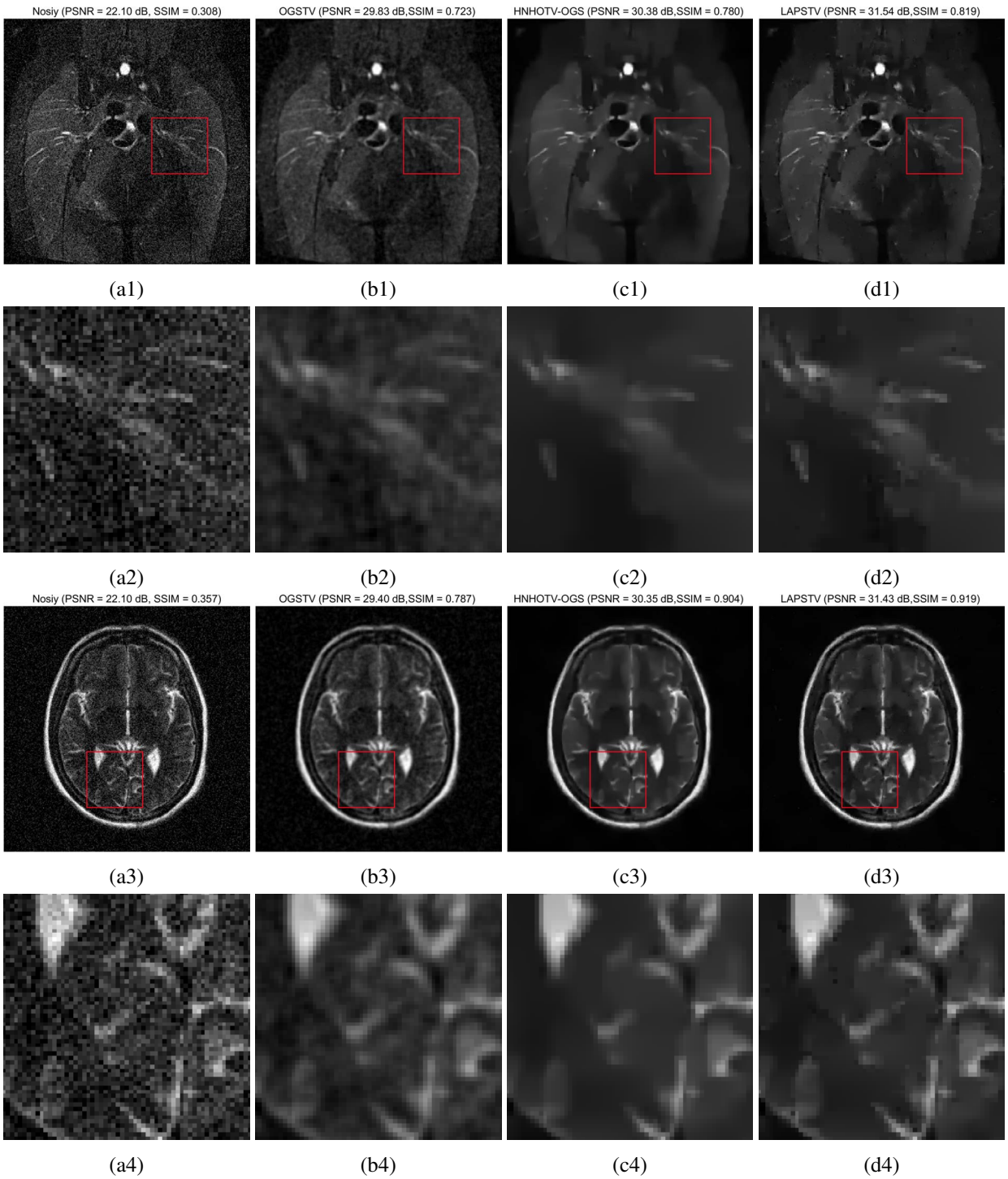

Fig. 3: *The first and third lines are the recovered results for "sacroiliac" and "head" with* $\sigma = 20$*, respectively, while the second and fourth lines show the fragments corresponding to the zoomed images. (a1)-(a4) noisy image, (b1)-(b4) OGSTV restored, (c1)-(c4) HNHOTV-OGS restored, (d1)-(d4) LAPSTV restored.*

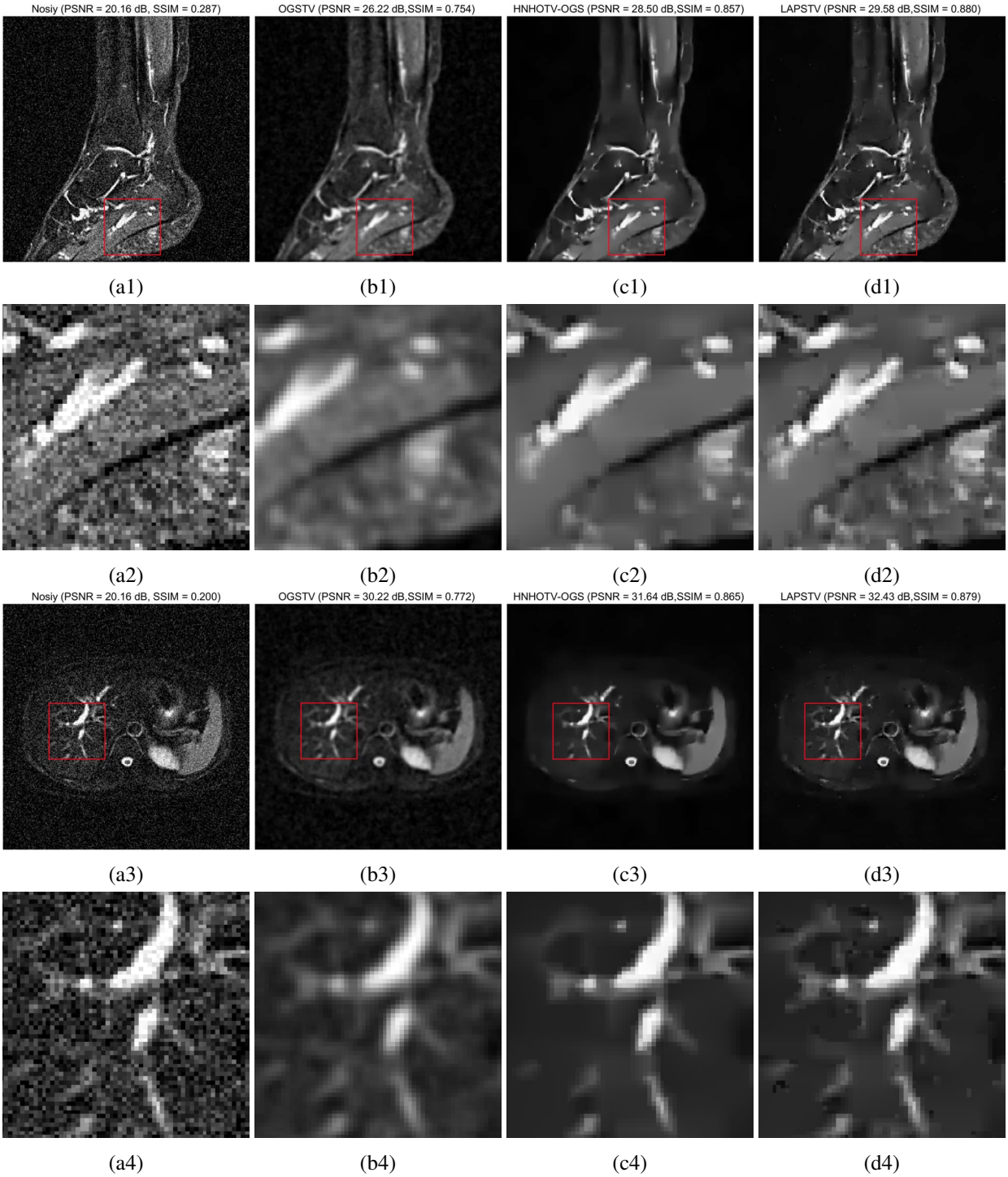

Fig. 4: *The first and third lines are the recovered results for "ankle" and "mrcp" with* $\sigma = 25$*, respectively, while the second and fourth lines show the fragments corresponding to the zoomed images. (a1)-(a4) noisy image, (b1)-(b4) OGSTV restored, (c1)-(c4) HNHOTV-OGS restored, (d1)-(d4) LAPSTV restored.*

comparable method to LAPSTV is HNHOTV-OGS. The restored images obtained using HNHOTV-OGS exhibit effective removal of staircase artifacts due to the inclusion of higher-order terms, which results in smoother images compared to LAPSTV. However, with the introduction of a hyper-Laplacian prior on the overlapping group sparsity term, LAPSTV is proposed to preserve important textures and edges in the images while effectively eliminating the staircase artifacts.

To facilitate a more comprehensive comparison of the denoising effects of each method, we utilize an image subtraction operation on the denoised images obtained from the three methods. This involves calculating the absolute value of the pixel-wise differences between the final denoised image and the clean image. Additionally, we plot the relative error curve, which quantifies the difference between the restored image and the original image after each iteration, using Eq. (21).

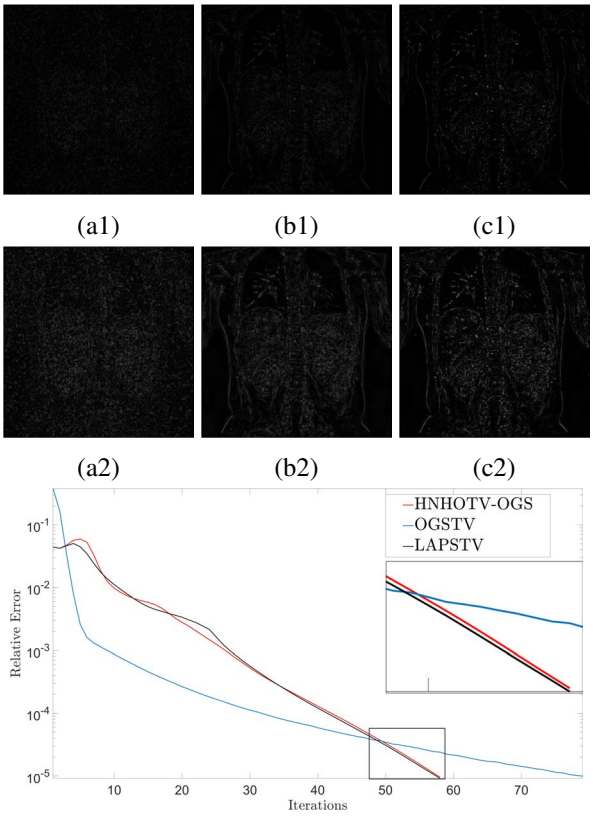

Fig. 5: *The first line is the differential images for "abdomen" (σ = 15), the second line shows the corrected differential images (contrast ratio: −40%). (a1)-(a2) differential images of OGSTV, (b1)-(b2) differential images of HNHOTV-OGS, (c1)-(c2) differential images of LAPSTV. The line chart shows the relative errors of the three methods as the number of iterations increases.*

As shown in Fig. 5-7, the differential images of LAPSTV exhibit the least noticeable differences compared to the other methods. In the relative error plot, each picture has a zoom-in patch to show the relative error curve changes of LAPSTV and HNHOTV-OGS. It can be observed that the curve of LAPSTV decreases slightly faster than that of HNHOTV-OGS at all three noise levels. Moreover, LAPSTV also yields higher PSNR and SSIM values compared to HNHOTV-OGS. Although the relative error curve of OGSTV shows the fastest decrease at noise levels σ=20 and 25, its denoising effect is comparatively poor.

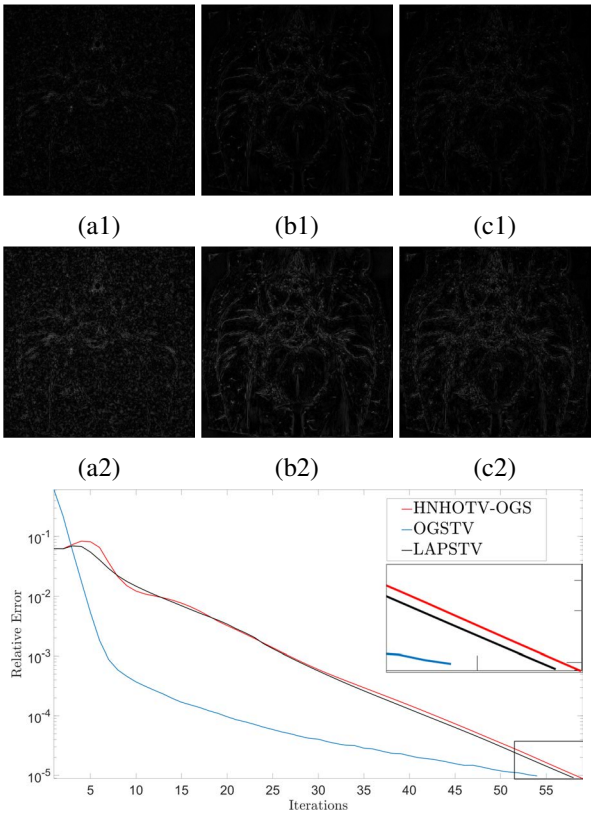

Fig. 6: *The first line is the differential images for "sacroiliac" (σ = 20), the second line shows the corrected differential images (contrast ratio: −40%). (a1)-(a2) differential images of OGSTV, (b1)-(b2) differential images of HNHOTV-OGS, (c1)-(c2) differential images of LAPSTV. The line chart shows the relative errors of the three methods as the number of iterations increases.*

VERIFY THE EFFECTIVENESS OF REMOVING STAIRCASE ARTIFACTS

In order to verify the effectiveness of removing the staircase artifacts by the hyper-Laplacian prior term with overlapping group sparse (the second term of the model), we named the nonconvex second-order TV obtained by removing the second term $\Phi(\nabla f)$ in the LAPSTV model (Eq. (9)) as LAPSTV-2nd term. It uses ADMM directly and IRL1 algorithm to solve

nonconvex l_p problems. The LAPSTV is compared with the LAPSTV-2nd term model and only the case of p=0.1 is considered.

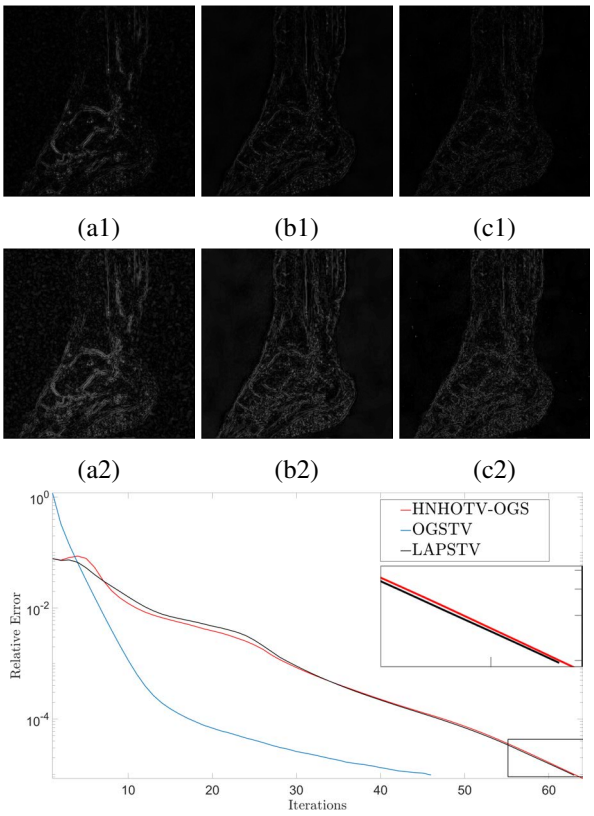

Fig. 7: *The first line is the differential images for "ankle" (σ = 25), the second line shows the corrected differential images (contrast ratio: −40%). (a1)-(a2) differential images of OGSTV, (b1)-(b2) differential images of HNHOTV-OGS, (c1)-(c2) differential images of LAPSTV. The line chart shows the relative errors of the three methods as the number of iterations increases.*

Fig. 8 and Fig. 9 show the PSNR and SSIM values of LAPSTV and LAPSTV-2nd term at σ=30 and 40, respectively. It can be seen that the PSNR and SSIM values of LAPSTV-2nd term without the second term decrease a lot. Fig. 10 is the restoration results of LAPSTV and LAPSTV-2nd term for "abdomen" at σ=30. Fig. 11 is the restoration results of LAPSTV and LAPSTV-2nd term for "sacroiliac" at σ=40. It can be observed from these figures that the denoising effect of the Lapstv-2nd term is not ideal and tends to magnify noise artifacts, while the LAPSTV recovery image smooths out these staircase artifacts.

PARAMETER SENSITIVITY ANALYSIS

The parameters that affect the performance mainly include the index (q) of the hyper-Laplace prior, the nonconvex l_p norm (p), the group size (k), and the number of MM iterations (N), these parameters need to be carefully tuned to get more accurate results. Therefore, we select two images, namely "abdomen" and "sacroiliac", to conduct tests with σ=20. This will help us demonstrate the sensitivity of the proposed model to these parameters.

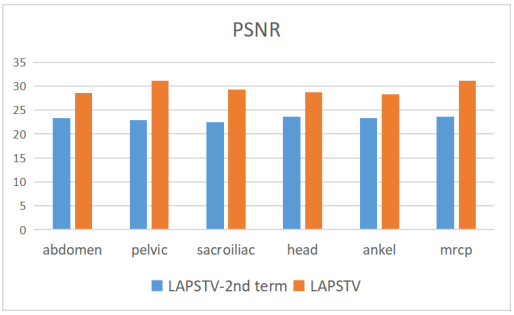

(a)

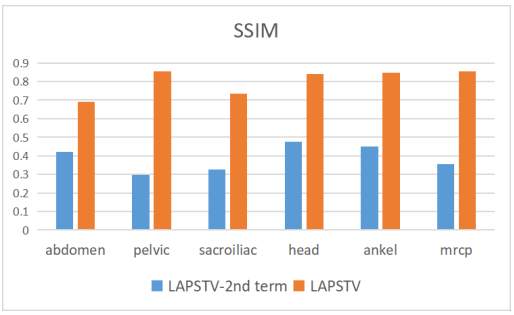

(b)

Fig. 8: *PSNR and SSIM values of LAPSTV-2nd item and LAPSTV denoising results when $\sigma = 30$.*

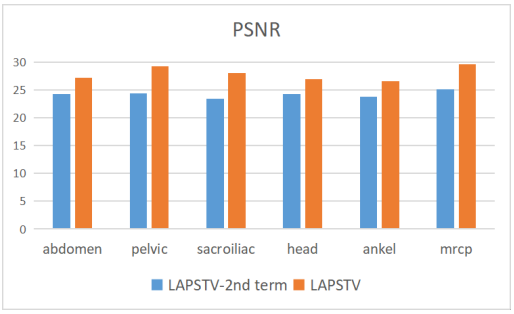

(a)

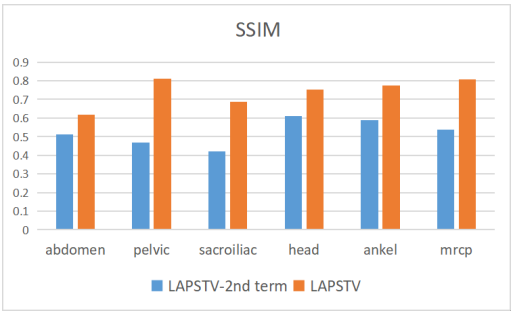

(b)

Fig. 9: *PSNR and SSIM values of LAPSTV-2nd item and LAPSTV denoising results when $\sigma = 40$.*

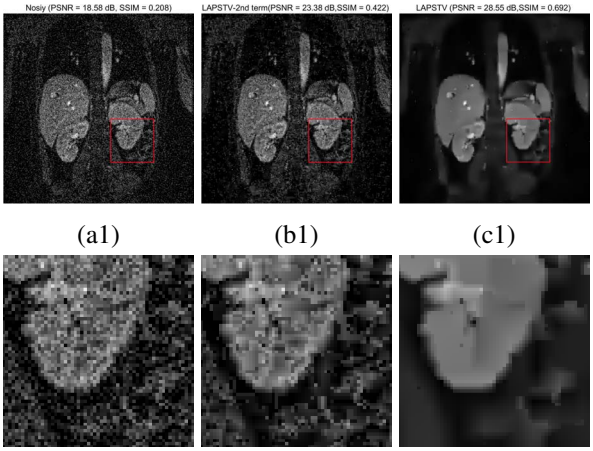

Fig. 10: *The first line is the recovered results for "abdomen" with* $\sigma = 30$*, the second line shows the fragments corresponding to the zoomed images. (a1)-(a2) noisy image, (b1)-(b2) LAPSTV-2nd item restored, (c1)-(c2) LAPSTV restored.*

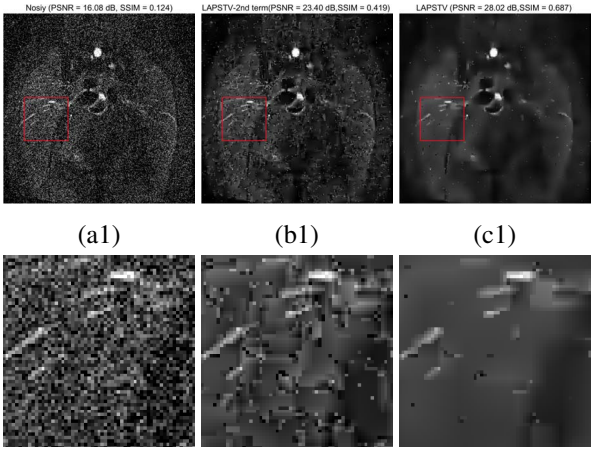

Fig. 11: *The first line is the recovered results for "sacroiliac" with* $\sigma = 40$*, the second line shows the fragments corresponding to the zoomed images. (a1)-(a2) noisy image, (b1)-(b2) LAPSTV-2nd item restored, (c1)-(c2) LAPSTV restored.*

Firstly, in order to test the sensitivity of iteration number N, other parameters are fixed. Table 4 shows the influence of different MM iteration numbers N on PSNR, SSIM, overall algorithm iteration number, and time, and the best result is obtained when N=5. The variation of the value of the group size K is important for the quality of the recovered image, and it can be obtained from Fig. 12 that when the group size K=3, the performance is the best, and if K value continues to increase, the curve will go downhill. The choice of p values for nonconvex l_p norm is crucial for restoring sharp and clear edges, $0 < p \leq 1$. In Fig. 13, the PSNR and SSIM values decrease as the p value increases from 0.1 to 1. Therefore, p = 0.1 can obtain the best PSNR and SSIM results.

The hyper-Laplace prior can well approximate the heavy-tailed distribution of natural image gradients, the overlapping group sparsity can alleviate staircase artifacts by introducing additional structural information, and the exponent q of the hyper-Laplace prior is used to measure the overlapping group sparsity of the image gradient ($0 < q < 1$). In Fig. 14, the optimal PSNR and SSIM values are obtained as the q value increases to 0.9. It is worth noting that when q=1, this item will be the special case OGS-TV.

Table 4: *Denoising results of different MM iterations (N) when* $\sigma = 20$

Image	N	PSNR	SSIM	Iter	Time(s)
abdomen	1	29.33	0.709	51	0.991
	5	31.28	0.819	58	2.593
	10	31.25	0.818	58	4.449
	100	31.24	0.818	58	37.328
sacroiliac	1	28.70	0.629	50	1.007
	5	31.54	0.819	58	2.580
	10	31.49	0.817	58	4.410
	100	31.47	0.816	58	37.421

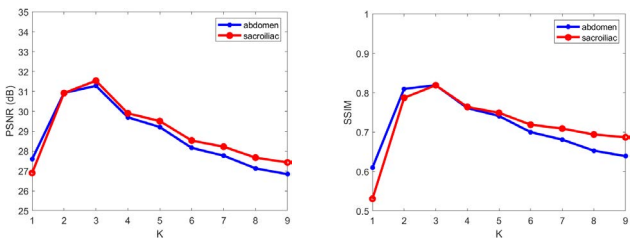

Fig. 12: *PSNR and SSIM values for images denoised by LAPSTV with different group sizes K when* σ *= 20.*

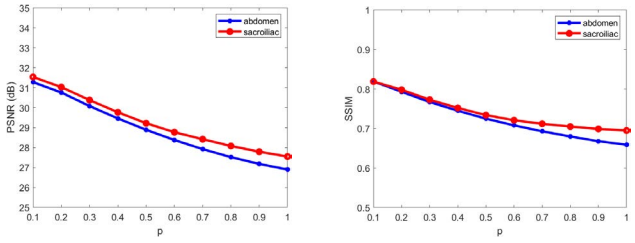

Fig. 13: *PSNR and SSIM values with different p when* $\sigma = 20$.

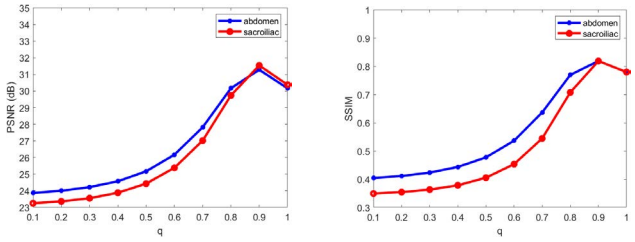

Fig. 14: *PSNR and SSIM values with different q when* $\sigma = 20$.

CONCLUSIONS

In this paper, we proposed a new MR images denoising method for recovering high quality image from a noisy image, We show that combining hyper-Laplace prior with the overlapping group sparse constraints and second-order nonconvex TV is a feasible solution to the magnetic resonance image denoising problem. This combination brings the ability to mitigate staircase artifacts and preserve important edges for effectively recoverying degraded image. Numerical experiments show that under the three different noise levels, the method is better than the other three different methods in terms of PSNR and SSIM. In future work, we plan to expand the ideal of the proposed method to blind denoising and reduce the model computation time.

ACKNOWLEDGMENTS

This work was supported in part by the Anhui Provincial Natural Science Foundation (No. 2208085MF168) and the University Synergy Innovation Program of Anhui Province (No. GXXT-2022-052).

REFERENCES

Adam T, Paramesran R (2019). Image denoising using combined higher order non-convex total variation with overlapping group sparsity. Multidim Syst Sign Process 30:503-27.

Al-Shayea T K, Mavromoustakis C X, Batalla J M, Mastorakis G, Mukherjee M, Pallis E (2020). A Novel Gaussian in Denoising Medical Images with Different Wavelets for Internet of Things Devices. Glob Commun Conf 100:1–6.

Bhadauria H S, Dewal M L (2013). Medical image denoising using adaptive fusion of curvelet transform and total variation. Comput Electr Eng 39:1451–60.

Boyd S, Parikh N, Chu E, Peleato B, Eckstein J (2011). Distributed optimization and statistical learning via the alternating direction method of multipliers. Found Trends Mach Learn 3:1–122.

Candes E J, Wakin M B, Boyd S P (2008). Enhancing sparsity by reweighted l_1 minimization. J Fourier Anal Appl 14:877–905.

Chan R H, Tao M, Yuan X (2013). Constrained total variation deblurring models and fast algorithms based on alternating direction method of multipliers. SIAM J Imaging Sci 6:680–97.

Chang Y, Yan L, Zhong S (2017). Hyper-laplacian regularized unidirectional low-rank tensor recovery for multispectral image denoising. Proc IEEE Conf Comput Vis Pattern Recog 2017:4260–8.

Chuan H, Chang-Hua H, ZHANG W, Biao S (2014). Box-constrained total-variation image restoration with automatic parameter estimation. Acta Automatica Sinica 40:1804–11.

El Hakoume A, Afraites L, Laghrib A (2022). An improved coupled PDE system applied to the inverse image denoising problem. Electron Res Arch 30:2618–42.

Gu X, Xue W, Sun Y, Qi X, Luo X, He Y (2023). Magnetic resonance image restoration via least absolute deviations measure with isotropic total variation constraint. Math Biosci Eng 20:10590-609.

Hadri A, Laghrib A, Oummi H (2021). An optimal variable exponent model for Magnetic Resonance Images denoising. Pattern Recognit Lett 151:302–9.

Hestenes M R (1969). Multiplier and gradient methods. J Optim Theory Appl 4:303–20.

Irum I, Shahid M A, Sharif M, Raza M (2015). A Review of Image Denoising Methods. J Eng Sci Technol Rev 8:41–8.

Jon K, Liu J, Wang X, Zhu W, Xing Y (2021). Weighted Hyper-Laplacian Prior with Overlapping Group Sparsity for Image Restoration under Cauchy Noise. J Sci Comput 87:1–32.

Jon K, Sun Y, Li Q, Liu J, Wang X, Zhu W (2021). Image restoration using overlapping group sparsity on hyper-laplacian prior of image gradient. Neurocomputing 420:57–69.

Kong J, Lu K, Jiang M (2017). A new blind deblurring method via hyper-Laplacian prior. Procedia Comput Sci 107:789–95.

Krishnan D, Fergus R (2009). Fast image deconvolution using hyper-Laplacian priors. Proc Adv Neural Inf Process Syst 22.

Liu R W, Shi L, Huang W, Xu J, Yu S C H, Wang D (2014). Generalized total variation-based MRI Rician denoising model with spatially adaptive regularization parameters. Magn Reson Imaging 32:702–20.

Liu G, Huang T Z, Liu J, Lv X G (2015). Total variation with overlapping group sparsity for image deblurring under impulse noise. PLoS One 10:e0122562.

Liu J, Huang T Z, Selesnick I W, Lv X G, Chen P Y (2015). Image restoration using total variation with overlapping group sparsity. Inf Sci 295:232–46.

Lyu Q, Lin Z, She Y, Zhang C (2013). A comparison of typical l_P minimization algorithms. Neurocomputing 119:413–24.

Mohan J, Krishnaveni V, Guo Y (2014). A survey on the magnetic resonance image denoising methods. Biomed Signal Process Control 9:56–69.

Rudin L I, Osher S, Fatemi E (1992). Nonlinear total variation based noise removal algorithms. Physica D 60:259–68.

Selesnick I W, Chen P Y (2013). Total variation denoising with overlapping group sparsity. IEEE Int Conf Acoust Speech Signal Process, 5696-700.

Shi M, Han T, Liu S (2016). Total variation image restoration using hyper-Laplacian prior with overlapping group sparsity. Signal Process 126:65–76.

Snehalatha S R (2020). Brain MRI Image Denoising Using Spectral Total Variation Denoising. Eur J Mol Clin Med 7:3044–51.

Sonia M S, Sumathi S (2022). A Comparative Analysis of Wavelet Transforms for Denoising MRI Brain Images. Int Conf Power, Energy, Control Transm Syst 103:1–5.

Tong C, Sun Y, Payet N, Ong S H (2012). A general strategy for anisotropic diffusion in MR image denoising and enhancement. Magn Reson Imaging 30:1381–93.

Wang Y, Yin W, Zeng J (2019). Global convergence of ADMM in nonconvex nonsmooth optimization. J Sci Comput 78:29–63.

Weaver J B, Xu Y, Healy Jr D M, Cromwell L D (1991). Filtering noise from images with wavelet transforms. Magn Reson Med 21:288–95.

Wu C, Tai X C (2010). Augmented Lagrangian method, dual methods, and split Bregman iteration for ROF, vectorial TV, and high order models. SIAM J Imaging Sci 3:300–39.

Zhu Y, Shen W, Cheng F, Jin C, Cao G (2020). Removal of high density Gaussian noise in compressed sensing MRI reconstruction through modified total variation image denoising method. Heliyon 6:e03680.

Zuo W, Meng D, Zhang L, Feng X, Zhang D (2013). A generalized iterated shrinkage algorithm for non-convex sparse coding. Proc IEEE Int Conf Comput Vis, 217–24.